Nanomaterials and Nanotechnology

OPEN ACCESS
ARTICLE

Plasmonics in Topological Insulators

Invited Review Article

Yi-Ping Lai[1], I-Tan Lin[1], Kuang-Hsiung Wu[2] and Jia-Ming Liu[1,*]

1 Electrical Engineering Department, University of California, Los Angeles, Los Angeles, California, USA
2 Department of Electrophysics, National Chiao-Tung University, Hsinchu, Taiwan
* Corresponding author E-mail: liu@ee.ucla.edu

Received 12 Feb 2014; Accepted 1 Apr 2014

DOI: 10.5772/58558

Abstract With strong spin-orbit coupling, topological insulators have an insulating bulk state, characterized by a band gap, and a conducting surface state, characterized by a Dirac cone. Plasmons in topological insulators show high frequency-tunability in the mid-infrared and terahertz spectral regions with transverse spin oscillations, also called "spin-plasmons". This paper presents a discussion and review of the developments in this field from the fundamental theory of plasmons in bulk, thin-film, and surface-magnetized topological insulators to the techniques of plasmon excitation and future applications.

Keywords Topological Insulator, Plasmons, Spin-orbit Interaction

1. Introduction

Topological insulators are a new class of materials that have strong spin-orbit coupling, leading to an insulating bulk state and an odd number of conducting edges or surface states protected by time-reversal symmetry. Topological insulators were first theoretically predicted and then experimentally measured in two-dimensional materials, such as HgTe/CdTe [1-3] and InAs/GaSb [4, 5] quantum well, and three-dimensional materials, such as Bi_2Se_3, Bi_2Te_3, and Sb_2Te_3 [6-11].

Plasmons are collective charge density oscillations, which occur due to long-range Coulomb interactions. Plasmonics in metals has flourished because of the ability that it offers to localize light on metal surfaces and interfaces in sub-wavelength regions. Plasmons in topological insulators show even more interesting characteristics. Their resonance frequencies are in the mid-infrared and terahertz spectral regions, which can be tuned by varying the Fermi level [12] or the wave vector. The backscattering of surface electrons by nonmagnetic impurities is prevented by the strong spin-orbit coupling [13], implying a long propagation length of plasmons. Moreover, due to spin-momentum locking, these plasmons are always accompanied by transverse spin oscillations and are thus also called "spin-plasmons" [14]. These features suggest that they have the potential for novel applications in plasmonics, spintronics and quantum computing. The surface conductivity of three-dimensional topological insulators is often overwhelmed by the bulk conductivity due to doping introduced by natural defects. Nanoscale topological insulators have a large surface-to-volume ratio, thus enhancing the contribution of the surface state. Plasmons in nanostructured topological insulators, such as thin films, multilayers, and nanoribbons, are essential for future applications. For the past few years, plasmonics in topological insulators has attracted great attention and

has been advancing at a rapid pace [15]. A thorough study and review in this field is necessary.

In this review, we summarize and discuss the recent theoretical and experimental progress of plasmonics in three-dimensional topological insulators. In section 2, the fundamental theory of plasmons in topological insulators is presented. In section 3, we focus on plasmons in topological insulator thin films. In section 4, plasmons in topological insulators subject to time-reversal symmetry breaking are discussed. In section 5, we review several methods of plasmon excitation. In section 6, we draw attention to some open questions and the future applications of plasmonics in topological insulators.

2. Plasmons on the surfaces of bulk topological insulators

In order to derive the plasmon modes on the surfaces of bulk topological insulators, we start from the surface Hamiltonian. The single-particle low-energy effective surface Hamiltonian of three-dimensional topological insulators can be expressed as [6]

$$H = \hbar v_{\mathrm{F}} (\boldsymbol{k} \times \boldsymbol{\sigma}) \cdot \hat{z} , \tag{1}$$

where $v_{\mathrm{F}} \simeq 6 \times 10^5$ m/s is the Fermi velocity, $\hat{z}$ is the direction of the surface normal, $\boldsymbol{\sigma}$ is the Pauli matrix vector, and $\boldsymbol{k}$ is the wave vector of a single electron.

Plasmons are collective charge oscillations which occur through long-range Coulomb coupling. For the plasmons on the surface of a topological insulator, the many-body Hamiltonian including the Coulomb interaction should be considered:

$$H = \hbar v_{\mathrm{F}} \sum_{\boldsymbol{k}} \psi_{\boldsymbol{k}}^{\dagger} (\boldsymbol{k} \times \boldsymbol{\sigma}) \cdot \hat{z} \psi_{\boldsymbol{k}.} + \frac{1}{2S} \sum_{\boldsymbol{q} \neq 0} V(q) \rho_{\boldsymbol{q}}^{\dagger} \rho_{-\boldsymbol{q}} , \tag{2}$$

where $\psi_{\boldsymbol{k}}^{\dagger}$ is the creation operator of an electron with momentum $\boldsymbol{k}$, S is the surface area of the topological insulator, $V(q) = e^2 / 2\varepsilon_{\mathrm{ave}} q$ is the two-dimensional Fourier transform of the Coulomb potential, and $\rho_{\boldsymbol{q}}$ is the density operator defined by $\rho_{\boldsymbol{q}} = \sum_{\boldsymbol{k}} \psi_{\boldsymbol{k}-\boldsymbol{q}}^{\dagger} \psi_{\boldsymbol{k}}$. It is not easy to solve Equation (2). The parameter $r_{\mathrm{s}} = e^2 / 4\pi\varepsilon_{\mathrm{ave}} \hbar v_{\mathrm{F}}$ represents the ratio of the characteristic Coulomb interaction energy to the kinetic energy, where $\varepsilon_{\mathrm{ave}} = (\varepsilon_{\mathrm{TI}} + \varepsilon_0)/2$ is the average electric permittivity of the topological insulator ($\varepsilon_{\mathrm{TI}}$) and the medium above its surface, which for the sake of simplicity is assumed here as being a vacuum (ε_0). If $r_{\mathrm{s}} \ll 1$, we can assume that the out-of-phase responses of electrons to the external field average out due to the random locations of the electrons in a large quantity; this assumption is called random phase approximation (RPA) [16]. For Bi_2Se_3, r_{s} is about 0.09. The RPA effective dielectric function for wave vector q and frequency ω is

$$\frac{\varepsilon_{\mathrm{RPA}}(q,\omega)}{\varepsilon_0} = 1 - V(q)\Pi(q,\omega) , \tag{3}$$

where $\Pi(q,\omega)$ is the two-dimensional non-interacting polarizability. The dispersion characteristics of plasmon modes are obtained by finding the zero of Equation (3).

Plasmons can be damped by single-particle excitations. Intraband and interband single-particle excitations are both prevented in the range of $v_{\mathrm{F}} q < \omega < 2\mu_{\mathrm{c}}/\hbar - v_{\mathrm{F}} q$, where μ_{c} denotes the chemical potential. Hence, the undamped plasmons only exist in this region. The white region in Figure 1 falls within this range. According to the quantum field calculations [14], the plasmons in this range are mainly made up of intraband transitions; therefore, the effect of the valence band is limited. The polarizability $\Pi(q,\omega)$ is real, which can be derived from Equation (1) under the assumption of low-temperature ($\hbar\omega \gg k_{\mathrm{B}} T$) [17] :

$$\begin{aligned} \Pi(q,\omega) = & -\frac{k_{\mathrm{F}}}{2\pi\hbar v_{\mathrm{F}}} + \frac{q^2}{16\pi\hbar\sqrt{\omega^2 - v_{\mathrm{F}}{}^2 q^2}} \\ & \times \left[G\left(\frac{2k_{\mathrm{F}} v_{\mathrm{F}} + \omega}{v_{\mathrm{F}} q} \right) - G\left(\frac{2k_{\mathrm{F}} v_{\mathrm{F}} - \omega}{v_{\mathrm{F}} q} \right) \right], \end{aligned} \tag{4}$$

where

$$G(x) = x\sqrt{x^2 - 1} - \ln\left(x + \sqrt{x^2 - 1} \right), \tag{5}$$

T is the temperature, and k_{F} is the Fermi wave vector. In the long-wavelength limit ($q \to 0$),

$$\Pi(q,\omega) = \frac{\mu_{\mathrm{c}} q^2}{4\pi\hbar^2\omega^2} . \tag{6}$$

The analytical form of the plasmon dispersion in this limit can be derived from Equations (3) and (6) [18] :

$$\omega = \sqrt{\frac{\mu_{\mathrm{c}} e^2}{8\pi\hbar^2 \varepsilon_{\mathrm{ave}}} q} . \tag{7}$$

As shown in Figure 1, the plasmon frequency is proportional to $\sqrt{q}$ in the long-wavelength limit, but it asymptotically approaches the upper boundary of the single-particle intraband excitation in the short-wavelength limit. Bi_2Se_3, Bi_2Te_3, and Sb_2Te_3 have large electric permittivities ($>100\varepsilon_0$), which lower the frequencies of the plasmons on the surfaces of these materials to the mid-infrared region. The retardation

effect becomes strong only when the momentum of the plasmon is comparable to that of a photon with $q = \frac{v_F e^2}{8\pi\hbar c^2 \varepsilon_0} k_F = 10^{-5} k_F$. The retardation effect exists only in a negligibly small region near the origin in Figure 1; therefore, we will only discuss non-retarded plasmons in this review.

Due to the spin-momentum locking, the flux density of charge particles ($\boldsymbol{j}$) and the spin density ($\boldsymbol{S}$) on the surface satisfy the relation [18]

$$\boldsymbol{j}(\boldsymbol{x}) = v_F \boldsymbol{S}(\boldsymbol{x}) \times \hat{\boldsymbol{z}} . \tag{8}$$

The charge density wave must be accompanied by a transverse spin wave, which is a unique characteristic of the plasmons in topological insulators, called "spin-plasmons". With the continuity equation, the ratio of the transverse spin amplitude (s_T) to the charge density amplitude (n) can be obtained:

$$\frac{s_T}{n} = \frac{\omega}{v_F q} = \sqrt{\frac{\mu_c e^2}{8\pi q \varepsilon_{ave} \hbar^2 v_F^2}} . \tag{9}$$

As shown in Figure 2, the amplitudes of the two waves are comparable; for the parameters used in Figure 1, the ratio is larger than one. Therefore, the coupled spin and charge density oscillations can be experimentally observed at the same time.

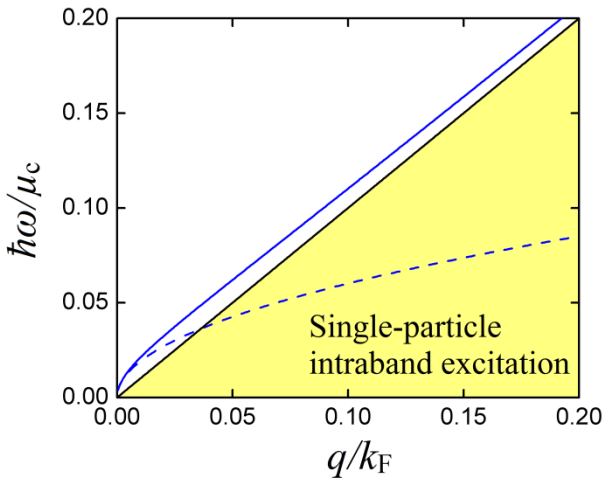

Figure 1. Plasmon dispersion and the region of single-particle intraband excitation (shaded) with $\mu_c = 0.1$ eV and $\varepsilon_{ave} = 50.5\varepsilon_0$ for Bi_2Se_3/vacuum interface. The exact dispersion solved by Equation (4) is shown by the blue solid curve, and the approximation given by Equation (7) in the long-wavelength limit is shown by the blue dash curve. The region of single-particle interband excitation ($\omega > 2\mu_c/\hbar - v_F q$) is much higher than the plasmon dispersion, thus beyond the scope of the figure.

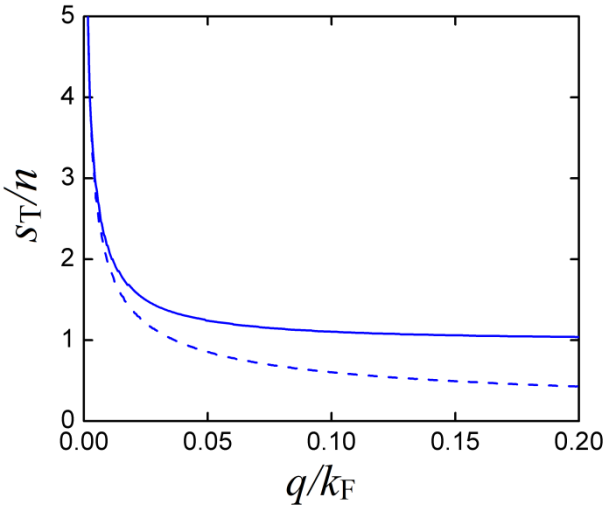

Figure 2. Ratio of the transverse spin amplitude to charge density amplitude calculated from the exact plasmon dispersion (solid) and the dispersion in the long-wavelength limit (dash) with the same parameters as used in Figure 1

3. Plasmons on the surface of topological insulator thin films

$V(q)$ in Equation (2) is modified for a topological insulator thin film where the plasmon modes on the top and bottom surfaces are unhybridized but Coulomb coupled. The RPA dielectric function becomes [19]

$$\frac{\varepsilon_{RPA}(q,\omega)}{\varepsilon_0} = \left[1 - V_{11}(q)\Pi_1(q,\omega)\right]\left[1 - V_{22}(q)\Pi_2(q,\omega)\right] - V_{12}^2(q)\Pi_1(q,\omega)\Pi_2(q,\omega), \tag{10}$$

where $\Pi_1(q,\omega)$ and $\Pi_2(q,\omega)$ are the polarizabilities of the top and bottom surfaces, respectively, $V_{11}(q)$ and $V_{22}(q)$ are the intralayer Coulomb potentials of the two surfaces; and $V_{12}(q)$ is the interlayer Coulomb potential :

$$V_{11,22} = \frac{e^2\left[(\varepsilon_{TI} + \varepsilon_{2,1})e^{qd} + (\varepsilon_{TI} - \varepsilon_{2,1})e^{-qd}\right]}{q\left[(\varepsilon_{TI} + \varepsilon_1)(\varepsilon_{TI} + \varepsilon_2)e^{qd} + (\varepsilon_{1,2} - \varepsilon_{TI})(\varepsilon_{TI} - \varepsilon_{2,1})e^{-qd}\right]}, \tag{11}$$

$$V_{12} = \frac{2e^2\varepsilon_{TI}}{q\left[(\varepsilon_{TI} + \varepsilon_1)(\varepsilon_{TI} + \varepsilon_2)e^{qd} + (\varepsilon_{1,2} - \varepsilon_{TI})(\varepsilon_{TI} - \varepsilon_{2,1})e^{-qd}\right]}, \tag{12}$$

where ε_1 and ε_2 are, respectively, the electric permittivities of the media above the top surface and below the bottom surface of the thin film, and d is the film thickness. There are two zeros in Equation (10), which are the optical plasmon mode and the acoustic plasmon mode.

The acoustic plasmon mode corresponds to out-of-phase charge oscillations and in-phase spin oscillations on the two surfaces [20]. The acoustic plasmon frequency is strongly suppressed by the large electric permittivity of the topological insulator because the out-of-phase charge

oscillations polarize the entire thin film. Outside the thin film, the electric field averages out so that only the spin oscillations can be observed. Thus, the acoustic plasmon mode is a "spin-like" mode. By contrast, the optical plasmon mode corresponds to in-phase charge oscillations and out-of-phase spin oscillations. The in-phase charge oscillations create a uniform electric field inside the thin film, reducing the effect of the large electric permittivity and raising the plasmon frequency to the terahertz region. Outside the thin film, the in-phase charge oscillations polarize the surrounding materials. Thus, the optical plasmon mode behaves as a "charge-like" mode instead. The dispersion characteristics of thin-film plasmons are shown in Figure 3. The plasmon frequencies are sensitive to qd and q/k_F. When qd or $q/k_F \gg 1$, the plasmon wavelength is much smaller than the film thickness or the distance between the intralayer electrons, meaning there is a weak interlayer Coulomb coupling. In this case, the plasmon dispersion curves approach that of the bulk topological insulator shown in Figure 1, as is seen in Figure 3.

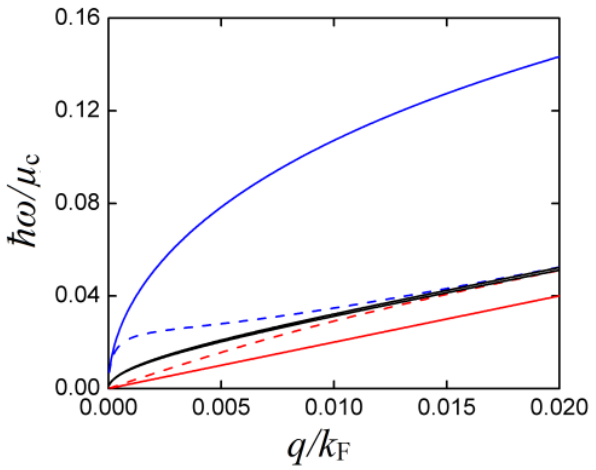

Figure 3. Optical (blue) and acoustic (red) plasmon dispersion characteristics for $k_F d = 1$ (solid) and $k_F d = 100$ (dash) with $\mu_c = 0.1$ eV, $\varepsilon_1 = \varepsilon_0$, $\varepsilon_2 = 10\varepsilon_0$ (Al_2O_3), and $\varepsilon_{TI} = 100\varepsilon_0$ (Bi_2Se_3). The decoupled plasmons on the top and bottom surfaces are also shown as a reference (black). The dispersion curves of the two decoupled plasmons are too close to be distinguished under the scale of the figure.

4. Plasmons in topological insulators with surface magnetization

4.1 Single topological insulator

The surface states of topological insulators are protected by the time-reversal symmetry. When the symmetry is broken by proximity to a magnetic material or by an externally applied magnetic field, the surface Hamiltonian acquires a Zeeman type of coupling term $m\sigma_z$ [21, 22]:

$$H = \hbar v_F (\boldsymbol{k} \times \boldsymbol{\sigma}) \cdot \hat{z} + m\sigma_z , \tag{13}$$

where the sign of m depends on the direction of the surface magnetization, and the size of the energy gap is $|2m|$. Here we assume that the magnetization is normal to the surface because magnetization in other directions only shifts the position of the Dirac point. The transverse Hall conductivity introduced by time-reversal symmetry breaking leads to a charge polarization induced by a magnetic field and a magnetization induced by an electric field, called the topological magnetoelectric effect [23, 24]. This effect can be described by a "θ term" in the constitutive relations,

$$\mathbf{D} = \varepsilon_{TI}\mathbf{E} - \frac{\theta}{\pi}\varepsilon_0 c\alpha\mathbf{B} , \tag{14}$$

$$\mathbf{H} = \frac{\mathbf{B}}{\mu_{TI}} + \frac{\theta}{\pi}\frac{\alpha\mathbf{E}}{c\mu_0} , \tag{15}$$

where $\theta = m\pi/|m|$ for a topological insulator with surface magnetization and $\theta = 0$ for a gapless topological insulator, α is the fine structure constant, μ_{TI} and μ_0 are the magnetic permeabilities of the topological insulator and a vacuum, respectively, c is the speed of light, $\mathbf{D}$ is the electric displacement, $\mathbf{E}$ is the electric field, $\mathbf{B}$ is the magnetic induction, and $\mathbf{H}$ is the magnetic field.

When the chemical potential is much larger than the surface energy gap but smaller than the bulk band gap ($E_{bulk} > \mu_c \gg |m|$), the surface conductivity can be approximated by using that of the gapless case. The longitudinal conductivity is directly related to the polarizability in Equation (4) by

$$\sigma(q,\omega) = i\omega\frac{e^2}{q^2}\Pi(q,\omega) . \tag{16}$$

The plasmon mode can be obtained from Equations (14)-(16) with appropriate boundary conditions. The plasmon mode is a hybrid mode, which is very different from the aforementioned transverse magnetic plasmon modes in gapless topological insulators. The ratio of the transverse magnetic component to the transverse electric component is independent of the gap size [25]:

$$\frac{E_{TM}}{E_{TE}} = \frac{\varepsilon_0 c\alpha\dfrac{\theta}{\pi}}{(\varepsilon + \varepsilon_{TI})\dfrac{\omega}{iq} + \sigma} , \tag{17}$$

where ε is the electric permittivity of the surrounding medium. The plasmon mode satisfies the condition

$$\left(-\frac{1}{\mu} - \frac{1}{\mu_{TI}} + \frac{i\sigma(q,\omega)\omega}{q}\right)\left(\varepsilon + \varepsilon_{TI} + \frac{i\sigma(q,\omega)q}{\omega}\right) = \left(\alpha\frac{\theta}{\pi}\right)^2\frac{\varepsilon_0}{\mu_0} , \tag{18}$$

where μ is the magnetic permeability of the surrounding medium. For Bi_2Se_3, $\varepsilon_{TI} = 100\varepsilon_0$, $\mu_{TI} \simeq \mu_0$, and $\mu_c \simeq 0.1$ eV, the plasmon dispersion is almost unaffected by the energy gap. When $\theta = 0$, Equation (18) corresponds to the plasmon condition for a gapless topological insulator. The dispersion characteristics of plasmon modes found under this condition are consistent with those obtained by finding the zero of Equation (3); then the plasmons become purely transverse magnetic modes again.

When (A) the chemical potential enters the bulk conduction band or (B) the chemical potential is comparable to the energy gap, we can rewrite Equation (18) as [26]

$$\left(-\frac{1}{\mu}-\frac{1}{\mu_{TI}}+\frac{i\sigma(q,\omega)\omega}{q}\right)(\varepsilon+\varepsilon_{TI})=\left(\alpha\frac{\theta}{\pi}\right)^2\frac{\varepsilon_0}{\mu_0}, \quad (19)$$

where the conductivity of the bulk conduction band is included in ε_{TI}. If $\sigma(q,\omega)$ is a positive imaginary, the first term on the left side is always negative. Then, the equation will have a solution only if $\varepsilon + \varepsilon_{TI} < 0$, which is similar to the surface plasmon conditions in metals. In case (A), a topological insulator can be modelled as a metal ; then, surface plasmon modes exist at the interface between a topological insulator and a dielectric medium such as a vacuum. In case (B), a topological insulator acts as a normal insulator; so surface plasmon modes exist at the interface between a topological insulator and a conductor such as a metal.

4.2 Multilayer topological insulators

To maximize the effect of time-reversal symmetry breaking, plasmons in multilayer topological insulators, as shown in Figure 4, are considered. In the long-wavelength limit ($q \to 0$), the conductivity is

$$\boldsymbol{\sigma}(\omega)=\begin{pmatrix}\sigma(\omega) & i\sigma_H(\omega)\\ -i\sigma_H(\omega) & \sigma(\omega)\end{pmatrix}, \quad (20)$$

where $\sigma_H(\omega)$ denotes the transverse conductivity Hall conductivity, derived from Equation (13) [27]:

$$\sigma_H(\omega)=i\frac{e^2m}{4\pi\omega\hbar^2}\ln\left|\frac{2\mu_c+\hbar\omega}{2\mu_c-\hbar\omega}\right|, \quad (21)$$

and $\sigma(\omega)$ is the longitudinal conductivity defined in Equation (16), which is a function of ω in the long-wavelength limit.

Assuming that the thickness, l_d, of each layer is much smaller than the plasmon wavelength and that charge oscillations are in phase, the overall electric permittivity of the system can be expressed as [27]

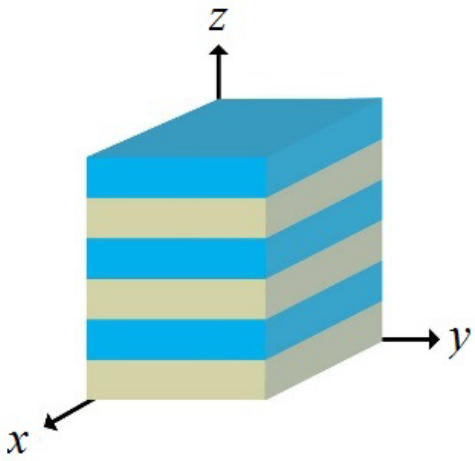

Figure 4. Multilayer structure composed of alternate stacking of topological insulators (gray layers) and dielectric insulators (blue layers)

$$\boldsymbol{\varepsilon}(\omega)=\begin{pmatrix}\varepsilon_{ave}+i\frac{\sigma(\omega)}{l_d\omega} & -\frac{\sigma_H(\omega)}{l_d\omega} & 0\\ \frac{\sigma_H(\omega)}{l_d\omega} & \varepsilon_{ave}+i\frac{\sigma(\omega)}{l_d\omega} & 0\\ 0 & 0 & \varepsilon_{ave}\end{pmatrix}, \quad (22)$$

where ε_{ave} is the average electric permittivity of the multilayer structure. The collective excitations can be determined by solving the wave equation

$$\boldsymbol{q}(\boldsymbol{q}\cdot\mathbf{E})-q^2\mathbf{E}+\omega^2\mu_{ave}\boldsymbol{\varepsilon}(\omega)\cdot\mathbf{E}=0, \quad (23)$$

where μ_{ave} is the average magnetic permeability of the multilayer structure.

As can be seen from Equations (22) and (23), only the in-plane polarization components of waves can "see" the effect of $\sigma_H(\omega)$. Assuming that both $\boldsymbol{E}$ and $\boldsymbol{q}$ are in-plane ($\boldsymbol{q}=q\hat{\boldsymbol{y}}$, $E_z=0$) without a loss of generality, Equation (23) becomes

$$\begin{pmatrix}\varepsilon_{ave}+i\frac{\sigma(\omega)}{l_d\omega}-\frac{q^2}{\omega^2\mu_{ave}} & -\frac{\sigma_H(\omega)}{l_d\omega}\\ \frac{\sigma_H(\omega)}{l_d\omega} & \varepsilon_{ave}+i\frac{\sigma(\omega)}{l_d\omega}\end{pmatrix}\begin{pmatrix}E_x\\ E_y\end{pmatrix}=0. \quad (24)$$

When $\sigma_H(q,\omega)=0$, the two components of the electric field are decoupled, which correspond to the longitudinal bulk plasmon mode and the transverse electromagnetic wave, shown by the dash curves in Figure 5. When $\sigma_H(q,\omega)\neq 0$, these two modes are hybridized, leading to two elliptically polarized eigenmodes, shown by the solid curves in Figure 5. When q is small, there is a large gap between these two eigenmodes, which is determined by

$\frac{\hbar\sigma_{\mathrm{H}}}{l_{\mathrm{d}}\varepsilon_{\mathrm{d}}}$, and each eigenmode is clearly separated from the decoupled plasmon mode and electromagnetic wave. By contrast, when q is large, the two eigenmodes separately approach the decoupled plasmon mode and electromagnetic wave while their gap increases, as seen in Figure 5.

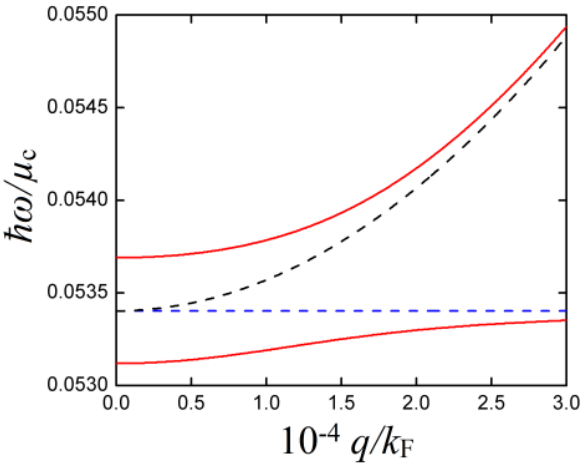

Figure 5. Dispersion characteristics of the hybrid modes with time-reversal symmetry breaking (red) and those of the decoupled longitudinal plasmon mode (black dash) and transverse electromagnetic wave (blue dash) without time-reversal symmetry breaking with $\mu_c = 0.1$ eV, $\varepsilon_{ave} = 50.5\varepsilon_0$, $\mu_{ave} = \mu_0$, $m = 0.2\mu_c$, and $v_F = 6\times10^5$ m/s

5. Excitation of plasmons

5.1 By grating structure

Plasmons in a topological insulator cannot be directly excited by light incident from free space because the momentum of photons is always smaller than that of plasmons. A grating structure of an appropriate period compensates for the momentum mismatch, which has been widely applied to the excitation of plasmons in graphene [28, 29] and metals, as shown in Figure 6. The first direct observation of plasmons in a topological insulator is done by illuminating Bi_2Se_3 nanoribbons with a terahertz light source [30], where the nanoribbons form the grating. Because the phase-matched plasmon frequency is determined by the grating period, this method shows less flexibility.

5.2 By optical spin injection

Plasmons in topological insulators are always accompanied by spin waves. Exciting plasmons by optical spin injection has been proposed [18], as shown in Figure 7. Spins carried by circular-polarized light may couple to the surface Dirac cone unequally; therefore, spins on the surface of a topological insulator can be controlled by the polarization of the incident light. Two cross-polarized optical beams of laser pulses generate a transient spin grating on the surface; the grating period is determined by the wavelength and the angle between the two incident beams [31, 32]. Plasmons are excited when the spin grating period matches the momentum of the plasmons.

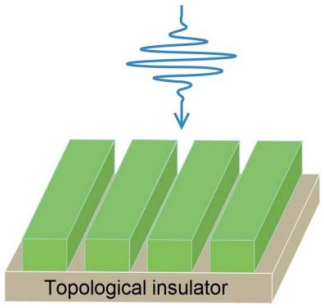

Figure 6. Illustration of plasmon excitation by a grating structure. The blue arrow denotes the incident light and the green stripes denote the grating structure.

Several theoretical works have shown the possibility of optical spin injection based on the symmetry considerations of the circular photogalvanic effect [33] and spin-dependent optical selection rules in ultrathin topological insulators [34]. Experiments, such as those using helicity-dependent photocurrents [35] and circularly polarized pump-probe spectroscopy [36], also confirm the feasibility of optical spin injection. However, the calculations including both spin-orbit coupling and Zeeman coupling show that the photocurrent of the surface state is dominated by the helicity-independent term [37], concluding that the experimentally observed helicity-dependent photocurrent [35] cannot be solely formed by the surface states. The Dirac surface states are found to extend deep into the materials. As a result, quantum interference between atomic layers should also be considered to calculate the full spin response [38]. The mechanism of light coupling to the surface states remains controversial; it needs more comprehensive theoretical and experimental studies.

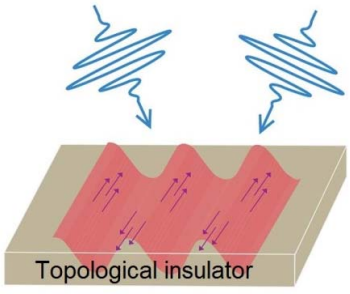

Figure 7. Illustration of plasmon excitation by optical spin injection. The two blue arrows are incident optical waves of the same frequency. The red wave is the spin grating, where the arrows indicate the direction of the spin.

5.3 By difference-frequency generation

Difference-frequency generation is another method of exciting plasmon waves with a high tunability in the plasmon frequency. Two obliquely incident pump waves excite plasmons at their frequency difference and momentum difference, as shown in Figure 8. Under the conditions that (1) the temperature is sufficiently low $k_B T \ll \mu_c$ such that electrons are degenerate, (2) the plasmon frequency is sufficiently high such that $\omega \gg q v_F, \gamma$, and (3) the frequencies of the two incident waves represented by ω_{pump} are comparable, the two-dimensional second-order nonlinear susceptibility is [39]

$$\chi^{(2)}(q,\omega) = \frac{e^3}{8\pi\hbar^2 \varepsilon_0 q \omega_{pump} \omega}\left(\frac{\pi}{2} + \tan^{-1}\frac{\omega_{pump} - 2v_F k_F}{\gamma}\right), \quad (25)$$

where γ is the plasmon decay rate. The value of this second-order nonlinear susceptibility is about 10^{-6}, which is four times higher than that of other quantum-well structures [40].

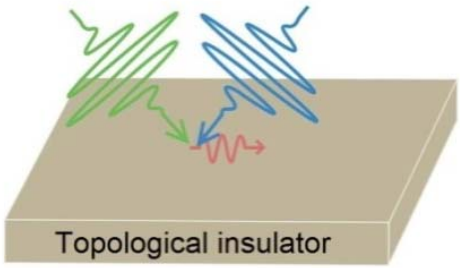

Figure 8. Illustration of plasmon excitation by difference-frequency generation. The blue and green arrows denote the two incident optical waves of different frequencies, and the red arrow represents the plasmon wave.

6. Conclusions

Many theoretical studies have revealed interesting properties of plasmonics in both bulk and nanoscale topological insulators. The broad range of plasmon frequencies in the mid-infrared and terahertz regions makes topological insulators a good candidate for generators, modulators, and detectors in this spectral range. The "spin-plasmon" nature enables spintronic applications, such as spin rectifiers [41]. Spin-plasmons only exist in the surface state, providing a method by which to probe the surface state regardless of its Fermi level.

The first experiment of plasmons in a topological insulator was done recently [30], which proved the existence of plasmons characterized by the surface Dirac cone. It also opens up some important questions, including the discrepancy in plasmon dispersions and the temperature-independent plasmon scattering rate. The next step is to experimentally investigate the spin oscillations that accompany the plasmon waves. More theoretical work on the effect of phonon coupling and massive two-dimensional electrons in the depletion layers underneath the surfaces [20] is also needed in order to explain the experimentally measured results.

7. Acknowledgment

This work was supported by U.S. Air Force AOARD under grant award no. FA2386-13-1-4022.

8. References

[1] Bernevig B A, Hughes T L and Zhang S C (2006) Quantum spin Hall effect and topological phase transition in HgTe quantum wells. Science 314: 1757-1761.

[2] Konig M, Wiedmann S, Brune C, Roth A, Buhmann H, Molenkamp L W, Qi X L and Zhang S C (2007) Quantum spin hall insulator state in HgTe quantum wells. Science 318: 766-770.

[3] Kane C L and Mele E J (2005) Z2 Topological Order and the Quantum Spin Hall Effect. Physical Review Letters 95: 146802.

[4] Knez I, Du R R and Sullivan G (2011) Evidence for Helical Edge Modes in Inverted InAs/GaSb Quantum Wells. Physical Review Letters 107: 136603.

[5] Liu C X, Hughes T L, Qi X L, Wang K and Zhang S C (2008) Quantum spin Hall effect in inverted Type-II semiconductors. Physical Review Letters 100: 236601.

[6] Zhang H J, Liu C X, Qi X L, Dai X, Fang Z and Zhang S C (2009) Topological insulators in Bi2Se3, Bi2Te3 and Sb2Te3 with a single Dirac cone on the surface. Nature Physics 5: 438-442.

[7] Xia Y, Qian D, Hsieh D, Wray L, Pal A, Lin H, Bansil A, Grauer D, Hor Y S, Cava R J and Hasan M Z (2009) Observation of a large-gap topological-insulator class with a single Dirac cone on the surface. Nature Physics 5: 398-402.

[8] Hsieh D, Qian D, Wray L, Xia Y, Hor Y S, Cava R J and Hasan M Z (2008) A topological Dirac insulator in a quantum spin Hall phase. Nature 452: 970-974.

[9] Chen Y L, Analytis J G, Chu J H, Liu Z K, Mo S K, Qi X L, Zhang H J, Lu D H, Dai X, Fang Z, Zhang S C, Fisher I R, Hussain Z and Shen Z X (2009) Experimental Realization of a Three-Dimensional Topological Insulator. Bi2Te3. Science 325: 178-181.

[10] Moore J E and Balents L (2007) Topological invariants of time-reversal-invariant band structures. Physical Review B 75: 121306(R).

[11] Fu L, Kane C L and Mele E J (2007) Topological insulators in three dimensions. Physical Review Letters 98: 106803.

[12] Hsieh D, Xia Y, Qian D, Wray L, Dil J H, Meier F, Osterwalder J, Patthey L, Checkelsky J G, Ong N P, Fedorov A V, Lin H, Bansil A, Grauer D, Hor Y S,

Cava R J and Hasan M Z (2009) A tunable topological insulator in the spin helical Dirac transport regime. Nature 460: 1101-1105.

[13] Zhang T, Cheng P, Chen X, Jia J-F, Ma X, He K, Wang L, Zhang H, Dai X, Fang Z, Xie X and Xue Q-K (2009) Experimental Demonstration of Topological Surface States Protected by Time-Reversal Symmetry. Physical Review Letters 103: 266803.

[14] Efimkin D K, Lozovik Y E and Sokolik A A (2012) Collective excitations on a surface of topological insulator. Nanoscale Research Letters 7: 1-10.

[15] Stauber T (2014) Plasmonics in Dirac systems: from graphene to topological insulators. Journal of Physics: Condensed Matter 26: 123201.

[16] Bohm D and Pines D (1951) A Collective Description of Electron Interactions. 1. Magnetic Interactions. Physical Review, 82: 625-634.

[17] Wunsch B, Stauber T, Sols F and Guinea F (2006) Dynamical polarization of graphene at finite doping. New Journal of Physics 8: 318.

[18] Raghu S, Chung S B, Qi X-L and Zhang S-C (2010) Collective Modes of a Helical Liquid. Physical Review Letters 104: 116401.

[19] Profumo R E V, Asgari R, Polini M and MacDonald A H (2012) Double-layer graphene and topological insulator thin-film plasmons. Physical Review B 85: 085443.

[20] Stauber T, Gomez-Santos G and Brey L (2013) Spin-charge separation of plasmonic excitations in thin topological insulators. Physical Review B 88: 205427.

[21] Liu C-X, Qi X-L, Zhang H, Dai X, Fang Z and Zhang S-C (2010) Model Hamiltonian for topological insulators. Physical Review B 82: 045122.

[22] Zhang F, Kane C L and Mele E J (2013) Surface State Magnetization and Chiral Edge States on Topological Insulators. Physical Review Letters 110: 046404.

[23] Qi X-L, Hughes T L and Zhang S-C (2008) Topological field theory of time-reversal invariant insulators. Physical Review B 78: 195424.

[24] Essin A M, Moore J E and Vanderbilt D (2009) Magnetoelectric Polarizability and Axion Electrodynamics in Crystalline Insulators. Physical Review Letters 102: 146805.

[25] Schutky R, Ertler C, Trugler A and Hohenester U (2013) Surface plasmons in doped topological insulators. Physical Review B 88: 195311.

[26] Karch A (2011) Surface plasmons and topological insulators. Physical Review B 83: 245432.

[27] Ye F and Liu C X (2013) Plasmon modes in magnetically doped single-layer and multilayer helical metals. Physical Review B 87: 115434.

[28] Gao W L, Shi G, Jin Z H, Shu J, Zhang Q, Vajtai R, Ajayan P M, Kono J and Xu Q F (2013) Excitation and Active Control of Propagating Surface Plasmon Polaritons in Graphene. Nano Letters 13: 3698-3702.

[29] Yan H G, Low T, Zhu W J, Wu Y Q, Freitag M, Li X S, Guinea F, Avouris P and Xia F N (2013) Damping pathways of mid-infrared plasmons in graphene nanostructures. Nature Photonics 7: 394-399.

[30] Di Pietro P, Ortolani M, Limaj O, Di Gaspare A, Giliberti V, Giorgianni F, Brahlek M, Bansal N, Koirala N, Oh S, Calvani P and Lupi S (2013) Observation of Dirac plasmons in a topological insulator. Nature Nanotechnology 8: 556-560.

[31] Koralek J D, Weber C P, Orenstein J, Bernevig B A, Zhang S C, Mack S and Awschalom D D (2009) Emergence of the persistent spin helix in semiconductor quantum wells. Nature 458: 610-613.

[32] Weber C P, Orenstein J, Bernevig B A, Zhang S C, Stephens J and Awschalom D D (2007) Nondiffusive spin dynamics in a two-dimensional electron gas. Physical Review Letters 98: 076604.

[33] Hosur P (2011) Circular photogalvanic effect on topological insulator surfaces: Berry-curvature-dependent response. Physical Review B 83: 035309.

[34] Lu H Z, Shan W Y, Yao W, Niu Q and Shen S Q (2010) Massive Dirac fermions and spin physics in an ultrathin film of topological insulator. Physical Review B 81: 115407.

[35] McIver J W, Hsieh D, Steinberg H, Jarillo-Herrero P and Gedik N (2012) Control over topological insulator photocurrents with light polarization. Nature Nanotechnology 7: 96-100.

[36] Li S, Huang H, Zhu W, Wang W, Chen K, Yao D-X, Wang Y, Lai T, Wu Y and Gan F (2011) Femtosecond laser-induced crystallization of amorphous Sb(2)Te(3) film and coherent phonon spectroscopy characterization and optical injection of electron spins. Journal of Applied Physics 110: 053523.

[37] Junck A, Refael G and von Oppen F (2013) Photocurrent response of topological insulator surface states. Physical Review B 88: 075144.

[38] Zhu Z H, Veenstra C N, Levy G, Ubaldini A, Syers P, Butch N P, Paglione J, Haverkort M W, Elfimov I S and Damascelli A (2013) Layer-By-Layer Entangled Spin-Orbital Texture of the Topological Surface State in Bi2Se3. Physical Review Letters 110: 216401.

[39] Yao X, Tokman M and Belyanin A (2014) Efficient Nonlinear Generation of THz Plasmons in Graphene and Topological Insulators. Physical Review Letters 112: 055501.

[40] Belkin M A, Capasso F, Belyanin A, Sivco D L, Cho A Y, Oakley D C, Vineis C J and Turner G W (2007) Terahertz quantum-cascade-laser source based on intracavity difference-frequency generation. Nature Photonics 1: 288-292.

[41] Appelbaum I, Drew H D and Fuhrer M S (2011) Proposal for a topological plasmon spin rectifier. Applied Physics Letters 98: 023103.